Combined Computational and Experimental Investigation of SO_x Adsorption on MgO

William F. Schneider,* John Li, and Kenneth C. Hass

Ford Research Laboratory, MD 3083/SRL, Dearborn, Michigan 48121-2053

Received: February 27, 2001; In Final Form: May 7, 2001

One of the main obstacles to the use of alkaline-earth-oxide-based NO_x adsorbents for emissions control is the ready poisoning of these materials by SO_x. To shed light on the mechanisms of poisoning, density functional theory (DFT) calculations and infrared spectroscopy experiments are used to study SO_x adsorption on MgO as a model alkaline earth oxide. DFT plane-wave, pseudopotential results are presented for SO_x adsorption on MgO(001) terraces and steps. Both SO_2 and SO_3 are found to exhibit both weakly bound physisorbed and strongly bound chemisorbed forms, with minimal activation barriers separating the two. Chemisorption is dominated by interactions between Lewis acidic sulfur and Lewis basic oxide anion sites to form surface sulfites and sulfates from SO_2 and SO_3, respectively. Within the generalized gradient approximation to DFT, the SO_2 adsorption energy ranges from 25 kcal mol^{-1} on terrace sites to 46 kcal mol^{-1} on lower-coordinated step edge sites; analogous SO_3 adsorption energies range from 49 to 76 kcal mol^{-1}. Surface sulfite is readily observed upon exposure of calcined MgO powder to SO_2 and produces vibrational signatures consistent with that calculated for chemisorbed SO_2. Sulfation is accomplished by exposure of the same powders to SO_2 and O_2 at elevated temperatures. Comparisons to calculated vibrational spectra indicate that both chemisorbed SO_2 and SO_3 are present under these conditions; further heating induces formation of a bulklike sulfate that is difficult to remove. The results demonstrate the high reactivity of SO_x toward metal oxides and illustrate the challenges in developing sulfur-resistant oxide-based NO_x traps.

Introduction

Reducing the concentration of NO_x in the exhaust of high efficiency lean-burn engines to an environmentally acceptable level is a major challenge facing the automotive industry. Although much effort has been expended in the development of catalysts capable of selectively reducing NO_x in an O_2-rich exhaust,[1] an alternative and promising technology is the use of a so-called NO_x trap.[2] These traps function by catalytically oxidizing and storing NO_x as a nitrate during lean operation of the engine and releasing and reducing it to N_2 during periodic rich, higher temperature excursions. The storage component of the traps is typically an alkaline earth oxide, and the net trapping reaction can be represented as

$$MO + 2NO_2 + {}^1/_2O_2 \rightarrow M(NO_3)_2 \quad (1)$$

Sulfur is a common trace contaminant in automotive fuels, and under lean operating conditions the NO_x traps are exposed to both SO_2 and SO_3. The formation of highly stable metal sulfites and sulfates competes with nitrate formation, eventually poisoning the trapping for NO_x adsorption

$$MO + SO_2 \rightarrow MSO_3 \quad (2)$$

$$MO + SO_3 \rightarrow MSO_4 \quad (3)$$

The thermodynamics of the bulk oxide, sulfate, and nitrate phases are reasonably well-established for the alkaline earth oxides. The molecular details of NO_x and SO_x adsorption and the extent to which reactions 1−3 are confined to the oxide surface or propagate into the bulk are less well understood. In this study, we use periodic supercell density functional theory (DFT)[3,4] calculations and Car-Parrinello molecular dynamics (CPMD)[5] to explore one aspect of this problem, specifically the initial adsorption of SO_2 or SO_3 on an otherwise clean alkaline earth oxide surface. We choose MgO to represent this class of oxides because the MgO surface has been widely studied and well characterized experimentally and computationally,[6] including several experimental[7−13] and computational[9,14,15] studies specifically of SO_x adsorption. Here, we consider the adsorbate structures and energetics of SO_2 and SO_3 on both the (001) basal plane and at monatomic step defects characteristic of MgO. We find that both SO_2 and SO_3 have high affinities for all MgO surfaces considered, and that the adsorbate structures and vibrational spectra follow trends easily understood in terms of the basicity of the surface oxide anions. Further, we report measurements of the vibrational spectra over a series of temperatures for MgO exposed to SO_2 in the absence and presence of O_2, and through comparison with computed vibrational spectra explain the observed adsorption patterns.

Computational Details

Periodic supercell, plane wave DFT calculations were performed using version 3.0 h of the parallelized CPMD code developed by J. Hutter and copyrighted by IBM, Armonk, New York. Nonlocal, norm-conserving pseudopotentials in the fully separable Kleinman-Blylander representation[16] were used for all ions. The analytic pseudopotential of Gonze et al.,[17,18] which treats all but the 3s electrons as core, was used for Mg, whereas numerical pseudopotentials of the Troullier-Martins type[19] were

* To whom correspondence should be addressed. E-mail: wschnei2@ford.com.

10.1021/jp010747r CCC: $20.00
Published on Web 06/22/2001

used for O and S. The first Brillouin zone was sampled at the Γ point; test calculations indicate that larger k-point sampling negligibly alters the structure and stability of the wide band gap materials considered here. As described in more detail below, MgO surfaces were described by slabs three or four atomic layers thick, with the bottom layer fixed at the bulk geometry and sufficient vacuum spacing included to isolate the slabs. Gradient-based energy minimizations were performed within the local density approximation (LDA).[20] Binding energies at the LDA minima were also evaluated within the generalized gradient approximation (GGA) using the PW91 functional.[21,22] Löwdin population analysis was performed on the converged wave functions by projecting them onto a double ζ plus polarization Slater local orbital basis. Harmonic vibrational frequencies were determined by two-sided numerical differentiation of the analytic gradients, including both adsorbate and surface atoms in the calculation.

To probe barriers to chemisorption and to assist in the location of adsorption sites on the MgO surfaces, Car-Parrinello molecular dynamics was used to simulate SO_x adsorption. The fictitious electron mass, which controls the coupling of the ionic and electronic degrees of freedom, and the dynamics time step were typically set to 2500 au and 10 au (0.242 fs) respectively, and provided both good energy conservation and little drift of the electronic kinetic energy. In a typical simulation, an SO_2 or SO_3 molecule was placed in an arbitrary location above an MgO surface and the ionic positions evolved using the LDA forces for up to 2 ps. The ionic velocities were initially assigned to some target temperature, typically 100 or 150 K. For some of the exothermic chemisorption reactions considered, the ionic velocities were periodically rescaled to the target temperature to remove excess thermal energy.

Experimental Details

SO_2 and SO_3 adsorption on MgO powder samples were performed in-situ using a high-vacuum IR cell equipped with CaF_2 windows. SO_2 (99.998%) from Matheson was used without further purification. High purity gases (O_2 99.998%, H_2 99.996%) were used to oxidize or reduce the sulfur species formed on the sample. MgO powders from Alfa-Aesar (99.998%) were pressed into gold wire mesh at 138 bar. The BET surface area of the initial MgO powders was measured as 30 m^2/g.

The experimental setup was as follows: A chromel−alumel thermocouple was spot-welded to a side of the gold mesh pressed with the MgO powder. The mesh was fixed to a portable probe arm, which also allowed resistive heating of the specimen. Spectra were recorded using a Mattson Cygnas 100 FTIR spectrometer with a resolution of 4 cm^{-1}. All spectra were recorded as single beam experiments and then ratioed to the initial, evacuated background spectrum.

MgO samples were heated to 600 °C and held for 180 min. The sample was then cooled to the adsorption temperature (25 °C or 350 °C). 1.0 Torr SO_2 was then leaked into the system and the IR spectra were recorded. The system could then either be heated or evacuated to study the desorption characteristics. SO_3 adsorption on MgO was studied by introducing 1.0 Torr SO_2 and 2.0 Torr of O_2 at the adsorption temperature. The sample was either heated or evacuated to study the oxidation and desorption characteristics. H_2 could also be introduced into the system for studying the reduction properties of the sulfur species at different temperatures.

Results and Discussion

MgO Bulk and Surface. MgO has the rock salt structure with an experimental lattice constant of 4.211 Å (corresponding to an Mg−O separation of 2.106 Å).[23] Using a 64-atom supercell and a plane wave cutoff of 70 Ry, the lattice constant is calculated to be 4.236 Å, which decreases by 0.001 Å upon increasing the cutoff to 100 Ry. Similar convergence is found for SO_2 and SO_3 gas-phase structures and adsorption energies, and for economy, we use a 70 Ry cutoff in all the work reported here.

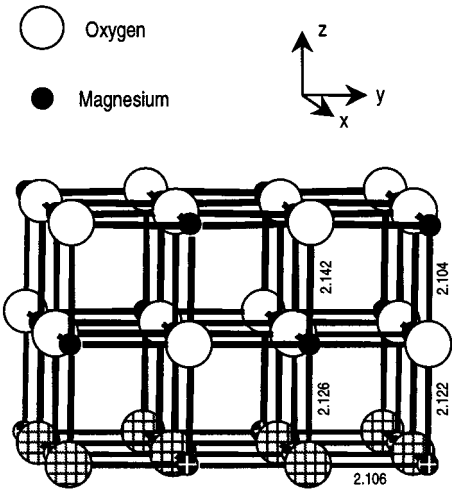

Figure 1. Side view of relaxed (001) surface model (distances in Å and angles in degrees). In-plane (x and y) repeat dimensions are 8.422 Å; vacuum (z) repeat dimension is 21.055 Å. Crosshatched atoms are fixed at their bulk locations.

The lowest energy surface of MgO is generally agreed to be the (001) basal plane of five-coordinate Mg and O atoms. To model the (001) surface, we use a 48 atom tetragonal supercell consisting of three layers of eight MgO formula units each (Figure 1) with an in-plane repeat dimension of 8.422 Å. The MgO slab is nominally 4.2 Å thick and is separated from its periodic images by a vacuum spacing four times that great. Similarly sized slabs have been successfully applied to H_2O adsorption on MgO(001).[24] In all simulations, ions in the bottom-most layer are fixed at the experimental bulk positions, whereas the upper two layers are unconstrained. After a brief run of low-temperature dynamics, the surface was relaxed to its minimum energy configuration. In agreement with earlier plane-wave calculations,[24,25] the relaxed surface is very slightly corrugated, with the outermost O atoms relaxing outward by 0.04 Å. Congruent with the relaxations found in the bulk system, the middle layer uniformly relaxes outward by 0.02 Å. The LDA surface energy is calculated to be 1.05 J m^{-2}, in good agreement with earlier theory and experiment.[26]

A monatomic step is a common defect on the (001) surface.[26] The step exposes both four-coordinate Mg and O atoms along its edge and six-coordinate atoms at its base and provides more reactive sites for sulfur adsorption. To model such a step, we examine the set of (10*n*) surfaces, in which monatomic steps are separated by terraces *n* rows wide. For odd and even *n* the surface is constructed within orthorhombic and monoclinic supercells, respectively. The supercells contain four layers of 2*n* MgO formula units each, with the bottom-most layer of ions again fixed at the bulk locations. In the direction parallel to the step (along the [100] vector) the cell dimension is again 8.422 Å, whereas the dimension between steps is determined by *n*, and the lattice constant in the "vacuum" direction is taken to be 2.5 × 8.422 Å, in rough correspondence with the vacuum spacing of the (001) model. The (103) supercell, which contains 48 atoms, is representative (Figure 2). Away from the step the

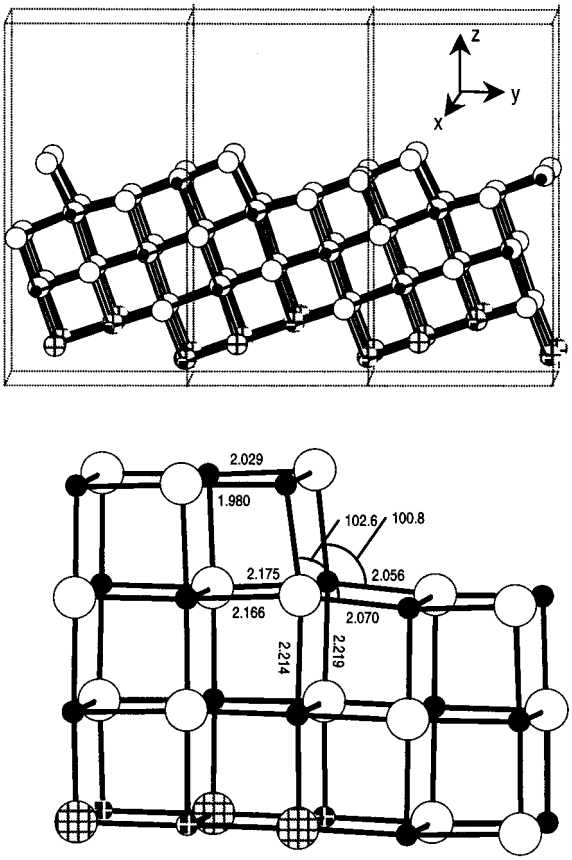

Figure 2. Side views of (103) surface model. Upper pane illustrates the surface terracing in the *y* direction; unit cell dimensions are 8.422 × 6.658 × 21.056 Å. Lower pane shows close-up of ion relaxation near a step (distances in Å and angles in degrees). Atom labeling is as in Figure 1, with crosshatched atoms fixed at their bulk locations.

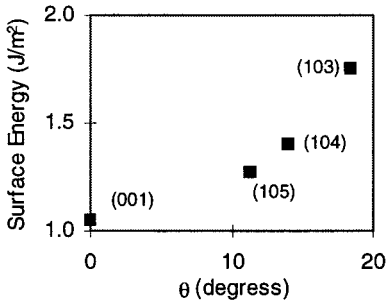

Figure 3. MgO basal and terraced surface energies (LDA) vs surface angle.

surface relaxes slightly upward, in line with the (001) results. At the step, the relaxation is more pronounced and follows that observed in earlier shell model[26] and supercell calculations: the six-coordinate ions at its base move outward toward the "vacant" ion row, increasing their separation from ions within the slab by up to 0.10 Å, whereas the four-coordinate ions at the step edge move toward the next row of surface ions. The result is an opening up of the inner step angle to slightly greater than 100°. These relaxations die off rapidly from the step, and are essentially unchanged from the (103) to (104) and (105) surfaces.

Following Tasker,[26,27] in Figure 3 the calculated surface energies are plotted against the surface angle $\theta = \arctan(1/n)$. The angle dependence of the surface energy reflects a combination of the step energy and the repulsive step-step interaction. The upward curvature of the surface energy indicates a larger step-step repulsion than found in shell-model calculations,[26,27]

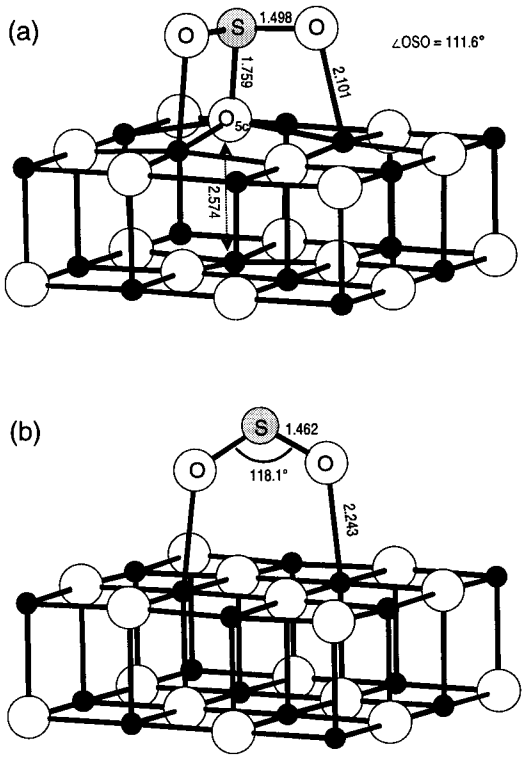

Figure 4. Chemisorbed (a) and physisorbed (b) SO_2 on (001) MgO (distances in Å). Bottommost MgO layers are hidden for clarity.

but extension of the simulations to larger values of *n* are necessary to quantify this effect.

SO_2 Adsorption. Despite numerous experimental[7−13] and theoretical[9,14,15] studies, the details of SO_2 adsorption on a fully dehydroxylated MgO surface are still not fully understood. Theoretical evidence for weak physisorption of SO_2 on the 5-coordinate basic sites of MgO(001) has been reported[14,15] and is consistent with low-temperature physisorption observed on several oxides.[10] Chemisorption of SO_2 on MgO to form surface sulfites is well-established experimentally,[7−13] but the structures of these adsorbates, and whether chemisorption is restricted to surface steps and kinks[14,15] or also occurs on the (001) basal plane, has received only limited consideration.[9]

Gas-phase SO_2 has a bent structure. The calculated LDA S−O bond length of 1.447 Å and O−S−O bond angle of 119.5° are in good agreement with the experimental values of 1.431 Å and 119°. In an initial dynamics simulations, SO_2 was placed approximately 4 Å above the relaxed MgO(001) surface and the system allowed to evolve, starting from a temperature of 100 K. The dipolar SO_2 molecule is attracted to the surface; as the SO_2 molecule approaches more closely this attraction increases and the system rapidly heats as the SO_2 is adsorbed. In less than 1 ps of simulation time, the SO_2 molecule is chemisorbed parallel to the surface, with the S atom above a five-coordinate surface O atom (O_{5c}) and the two SO_2 oxygens above adjacent surface Mg (Mg_{5c}). This chemisorbed state is unaltered by further annealing at 150 K. Relaxation yields the minimum energy structure shown in Figure 4a.

SO_2 is a powerful Lewis acid, and the MgO−SO_2 bonding is dominated by interaction with a basic surface oxide anion. As shown in Figure 4a, this interaction is quite strong, raising O_{5c} above the surface plane by nearly 0.5 Å to produce an S−O_{5c} bond only 1.76 Å long. Chemisorption lengthens the original S−O bonds by 0.05 Å and decreases the O−S−O angle to 111.6° so that the final structure resembles a distorted trigonal

TABLE 1: Selected Bond Lengths (Å), Gross Löwdin Charges, and Adsorption Energies (kcal mol^{-1}) of SO_2 and SO_3 Adsorbates

	$S-O_{surface}$	S−O	SO_x charge	E_{ads} LDA	E_{ads} GGA
		MgO(001) + SO_2			
physisorbed	2.243[a] (2)	1.462 (2)	0.094	−13.6	−5.1
chemisorbed	1.759	1.498 (2)	−0.341	−38.6	−24.8
		MgO(103) + SO_2 [b]			
$S^{(4)}O^{(1)}O^{(3)}$	1.655	1.536, 1.505	−0.401	−61.8	−45.8
$S^{(3)}O^{(3)}O^{(2)}$	1.658	1.517, 1.510	−0.403	−59.1	−45.8
$S^{(1)}O^{(1)}O^{(3)}$	1.706	1.557, 1.466	−0.398	−59.6	−43.3
$S^{(1)}O^{(1)}O^{(2)}$	1.762	1.548, 1.503	−0.363	−52.4	−31.2
$S^{(2)}O^{(1)}O^{(2)}$	1.695	1.513, 1.499	−0.330	−46.2	−28.9
$S^{(2)}O^{(3)}O^{(2)}$	1.780	1.491, 1.499	−0.299	−33.8	−18.3
		MgO(001) + SO_3			
physisorbed	2.292[a] (2)	1.443 (2), 1.435	0.142	−12.3	−4.2
chemisorbed	1.652	1.458, 1.469, 1.467	−0.522	−65.2	−48.6
		MgO(103) + SO_3 [b]			
$S^{(3)}O^{(3)}O^{(3)}O^{(4)}$	1.578	1.499, 1.440, 1.498	−0.572	−94.9	−76.3
$S^{(4)}O^{(4)}O^{(4)}O^{(3)}$	1.568	1.477, 1.469, 1.478	−0.565	−90.8	−74.7
$S^{(1)}O^{(1)}O^{(1)}O^{(2)}$	1.634	1.479, 1.486, 1.464	−0.477	−71.5	−48.6

[a] Distance from adsorbate O to surface Mg. [b] Numbers refer to locations of atoms in rows above (103) surface, as identified in Figure 6.

SO_3^{2-} (sulfite) anion. From the Löwdin population analysis, approximately 0.34 electrons are transferred from the surface to the adsorbed SO_2, confirming the anionic character of the final adsorbate. The increase in S−O bond lengths and closing of the O−S−O angle allow a secondary, weaker Lewis interaction between each of the basic SO_2 oxygens and an acidic Mg_{5c} to be formed. The two Mg_{5c} ions participating in this interaction are drawn more than 0.10 Å above the surface and the final Mg_{5c}−O distances are only 2.10 Å. Although the distortions of the MgO surface directly beneath the adsorbed SO_2 are pronounced, these distortions die off over a very short range. Thus, SO_2 is found to form a highly localized and strongly bound (25 kcal mol^{-1} at the GGA level, Table 1) chemisorbed complex on MgO(001) that can best be described as a surface sulfite (**1**). Its calculated structure and SO_2 adsorption energy are entirely consistent with the recent DFT results of Rodriguez et al.[9]

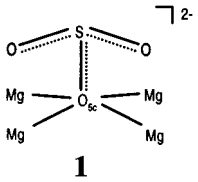

1

Embedded cluster Hartree−Fock calculations that explicitly include only a single O^{2-} ion and its five neighboring Mg^{2+} fail to reproduce this strongly chemisorbed state,[15] but rather predict SO_2 to be physisorbed on MgO(001) through the SO_2 oxygen.[14] We have located a similar physisorbed state (Figure 4b) in which the SO_2 adsorbate sits approximately 2.24 Å above an essentially unperturbed MgO(001) surface with a GGA binding energy of 5 kcal mol^{-1}. To explore the kinetic stability of the physisorbed SO_2, the fully relaxed structure was annealed in approximately 50 K steps of 0.5 to 1 ps in length to approximately 250 K, at which temperature the physisorbed SO_2 "tipped over" into the chemisorbed form. Although accurate estimates are not possible from these limited dynamics simulations, the results suggest a small but significant barrier between physi- and chemisorbed SO_2 of the order $k_BT \approx 0.5$ kcal mol^{-1}. Pacchioni et al.[14] identified two other weakly bound configurations of SO_2 on the MgO(001) surface, involving mono- and bidentate coordination of SO_2 to a single Mg_{5c}; we find both of these to be even more weakly bound than the physisorbed structure shown in Figure 4b and from dynamics simulations to readily convert to chemisorbed SO_2 at very low temperature. SO_2 can weakly and nonspecifically physisorb on MgO(001) but only a small activation barrier separates this physisorbed state from a strong and distinct chemisorbed state. Because of this very small barrier, experimental observations[10] of physisorbed SO_2 most likely correspond to adsorption on top of chemisorbed SO_2 rather than direct physisorption on the MgO surface.

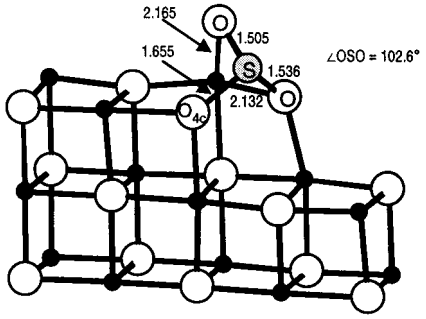

Figure 5. Lowest energy chemisorption site of SO_2 at a monatomic step edge (distances in Å). Only ions nearest to adsorption site are shown for clarity.

A monatomic step provides a number of additional oxide ion sites for SO_2 adsorption beyond the terrace site discussed above, including four-coordinate O_{4c} at the step edge and five-coordinate O_{5c} at the top and bottom of the step. Following a strategy as above, an SO_2 molecule was placed in an arbitrary location above the step edge of the MgO(103) surface and allowed to evolve from an initial temperature of 100 K. Chemisorption occurs spontaneously at the step edge; relaxation of the adsorbate yields the structure shown in Figure 5. As on the terrace, the primary adsorbate interaction is between the S atom and an edge O_{4c} ion to produce an approximately pyramidal sulfite structure, with secondary interactions with neighbor Mg ions. The lower coordination of the edge ions makes them more basic and thus more reactive toward SO_2. From the Löwdin analysis charge transfer from MgO to the adsorbate is an additional 0.06 electrons over the (001) surface; the additional charge-transfer results in a further lengthening of the S−O bonds (to >1.5 Å) and closing of the O−S−O angle (to 103°). The resulting surface sulfite is more nearly symmetric and SO_2 more strongly bound (by 21 kcal mol^{-1} at the GGA level, Table 1) than on the (001) surface.

A useful way to categorize this and other chemisorption sites on the (103) surface is in terms of the occupation of "virtual" lattice sites by adsorbed S and O. As shown in Figure 6, the (103) surface presents four unique rows of virtual sites. The adsorbed S center can be located above an O ion in any of these rows, with the corresponding SO_2 oxygen in the same or adjacent rows. Table 1 lists the calculated adsorption energies for six different adsorption sites labeled by the rows in Figure 6 [e.g., the site in Figure 5 is labeled "$S^{(4)}O^{(1)}O^{(3)}$"]. In the first three adsorption geometries, the SO_2 sulfur is bound at the step edge to four-coordinate oxygen, giving these three distinctly higher adsorption energies. The higher binding energies are also reflected in greater charge transfer to the SO_2 adsorbate. In the remaining three, sulfur is bound to six-coordinate oxygen, and the adsorption energies and charge-transfer approach that on the (001) terrace. The weakest adsorption geometry [$S^{(2)}O^{(3)}O^{(2)}$] is nearly isoenergetic and isostructural with SO_2 on the (001)

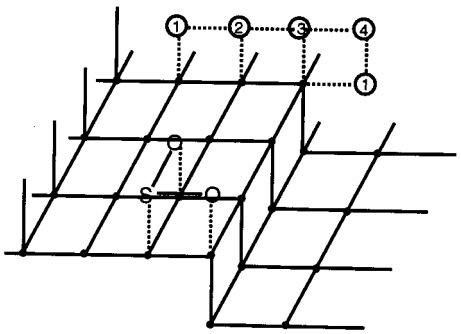

Figure 6. Schematic (103) surface showing four unique ion rows for adsorption.

surface (Figure 4a), suggesting that the three-row-wide terrace-step reasonably represents the full range of adsorption near a step. SO_2 adsorption was considered on the (104) stepped surface as well; for the two cases considered, the adsorbate structures and energetics were essentially identical to the corresponding (103) results. Embedded cluster calculations have been used to consider adsorption at a step and do reproduce the primary $S-O_{4c}$ interaction found here. The cluster calculations miss the secondary interactions with lattice Mg, and as a result get structures and binding energies in poor agreement with those reported here.[14]

In summary, on hydroxyl-free MgO, SO_2 at low coverage chemisorbs exclusively on lattice O ions to form surface sulfites.

SO_3 Adsorption. Because of the high reactivity of SO_3, its direct adsorption on MgO has been studied only to a limited extent.[28] Rather, sulfation of MgO is typically accomplished by exposure of MgO to SO_2 and excess O_2[11] or by decomposition of adsorbed SO_2.[9] The nature of the surface species thus formed is not well-known.

Gas-phase SO_3 has a trigonal planar geometry. The LDA S−O bond length of 1.436 Å slightly overestimates the experimental value of 1.42 Å, similar to SO_2. Like SO_2, SO_3 is found to weakly physisorb to MgO(001) in a perpendicular geometry akin to that in Figure 4b, with little distortion of the SO_3 structure. This physisorbed state readily converts into a chemisorbed one in molecular dynamics simulations performed at 100 K. Further relaxation gives the final chemisorbed SO_3 structure shown in Figure 7a. SO_3 is even more oxophilic than SO_2; chemisorption is again dominated by the $S-O_{5c}$ interaction, which raises O_{5c} 0.3 Å above the surface plane. The S center becomes significantly pyramidalized and the S−O bonds lengthened so that the SO_3 plus O_{5c} form a nearly tetrahedral sulfate-like structure (**2**). Again secondary interactions with Mg_{5c}

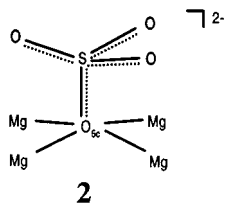

2

lock the SO_3 into a specific surface orientation with two of the O atoms aligned above Mg_{5c}. Approximately 0.52 electrons are transferred from the surface to the adsorbate according to the Löwdin charge analysis, and this pronounced charge transfer is reflected in a GGA chemisorption energy of 49 kcal mol^{-1}, nearly 25 kcal mol^{-1} greater than that for SO_2 on the same surface (Table 1).

SO_3 exhibits a strong preference for chemisorption at edge atoms of the (103) surface. Figure 7b shows the lowest energy

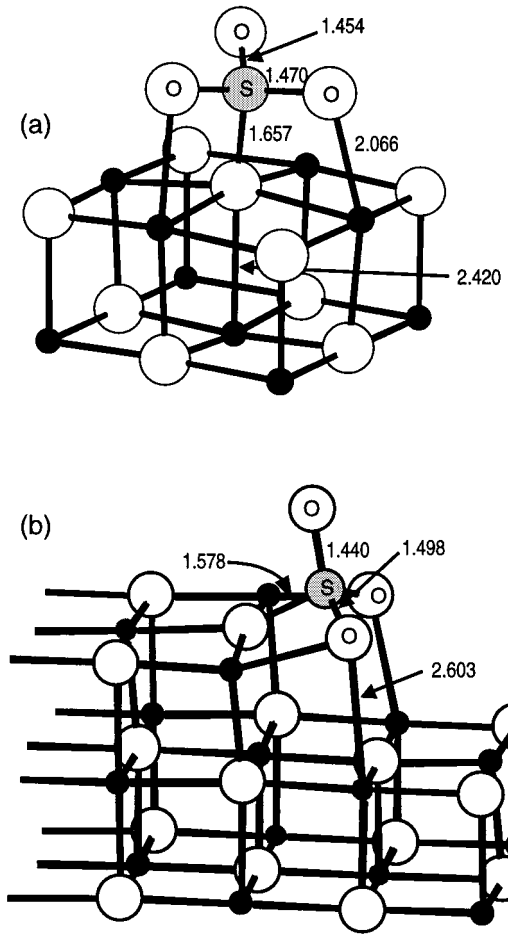

Figure 7. SO_3 chemisorbed on the (001) (a) and (103) (b) MgO surfaces (distances in Å). Only ions nearest to adsorption sites are shown for clarity.

adsorbate geometry found here, in which the S atom is bound to an edge O_{4c} and two of the three O atoms are fit into the crease of the step, thus coordinating to two surface Mg each. The S center is again nearly tetrahedral and clearly sulfate-like. The newly formed $S-O_{4c}$ bond is shorter than the same bond on the (001) surface by 0.08 Å. This decrease is reflected in a nearly 30 kcal mol^{-1} increase in adsorption energy at the step vs the terrace (Table 1). The variety of SO_3 adsorption sites on the (103) surface is even greater than with SO_2, all deriving from the same primary $S-O_s$ interaction and the same general sulfate adsorption mode. Table 1 includes results for two others, labeled using the notation of Figure 6. One of these [$S^{(4)}O^{(4)}O^{(4)}O^{(3)}$] is also located along the step edge; while the SO_3 location is quite different, the adsorption energetics are quite similar to that of Figure 7b. The other [$S^{(1)}O^{(1)}O^{(1)}O^{(2)}$] is further removed from the step edge and approaches the geometry and adsorption energy found on the (001) surface.

Similar to SO_2, on the hydroxyl-free MgO surface SO_3 chemisorbs exclusively at O_s sites to form strongly bound surface sulfates.

Vibrational Spectra. Vibrational spectroscopy has been widely used to characterize sulfur oxide adsorption on MgO, and comparison with calculated spectra can shed some light on the observed products. Table 2 contains calculated harmonic vibrational stretch frequencies for SO_2, SO_3, and several of the adsorbate structures reported above. We focus on the adsorbate stretch frequencies only because these are the modes most readily distinguished experimentally.

TABLE 2: Calculated Harmonic Stretch Vibrational Frequencies and Corresponding Features in Experimental Spectra (cm^{-1})

	calc'd		exp't	
	ν_{asym}	ν_{sym}	ν_{asym}	ν_{sym}
SO_2	1318	1119	1361[a]	1151[a]
MgO(001) + SO_2, physisorbed	1251	1075	1339[b]	1132[b]
MgO(001) + SO_2, chemisorbed	1096	1017	1030−1050	950−960
MgO(103) + SO_2, chemisorbed	1041	962	"	"

	$\nu_{e'}$	$\nu_{e'}$	$\nu_{a'}$	$\nu_{e'}$	$\nu_{e'}$	$\nu_{a'}$
SO_3	1345	1345	1026	1330[a]	1330[a]	1069[a]
MgO(001) + SO_3, chemisorbed	1239	1204	999	1260	1100	930
MgO(103) + SO_3, chemisorbed	1274	1094	955	"	"	"

[a] Ref 29. [b] Experimentally observed physisorption, likely on a modifed MgO surface.

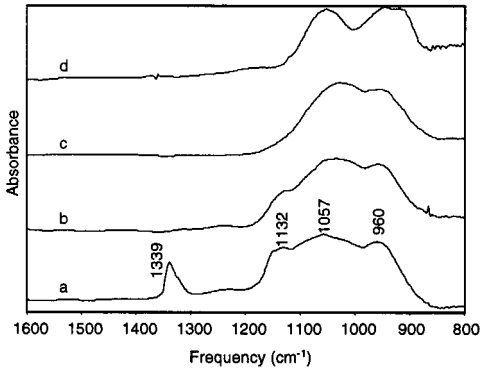

Figure 8. Observed vibrational spectra of SO_2-exposed precalcined MgO: (a) after exposure at 25 °C; (b) after evacuation at 25 °C; (c) after further evacuation at 100 °C; (d) after exposure at 350 °C.

The asymmetric (1361 cm^{-1}) and symmetric (1151 cm^{-1}) stretch fundamentals of gas-phase SO_2 are separated by 210 cm^{-1}.[29] The LDA frequencies underestimate the experimental fundamentals by approximately 3% and this splitting by 5% (Table 2). These modes are calculated to red-shift by 67 and 44 cm^{-1}, respectively, when SO_2 is physisorbed on MgO(001) (Figure 4b). Chemisorption on the (001) surface causes a much more pronounced red shift (>200 cm^{-1}) of the asymmetric and weaker red shift (~100 cm^{-1}) of the symmetric stretches, so the two bands are separated by only 80 cm^{-1}. At a step edge (Figure 5), both modes are further red-shifted by ~50 cm^{-1} (Table 2), whereas the same separation is maintained.

Vibrational spectra were collected at 25 and 350 °C for SO_2 adsorbed on MgO pretreated at 600 °C in a vacuum. At 25 °C (Figure 8a), strong absorption features are observed at 1339, 1132, 1057, and 960 cm^{-1}, along with a negative band at 3750 cm^{-1} reflecting perturbations by adsorbed SO_2 of residual surface hydroxyl groups.[10] Upon evacuation at 25 °C for 180 min (Figure 8b) and further at 100 °C (Figure 8c) the 1339 and 1132 cm^{-1} bands diminish in intensity and eventually disappear, consistent with their assignment to the asymmetric and symmetric stretches of weakly physisorbed SO_2.[7,10,13] These bands are red shifted by 10−20 cm^{-1} from those of gas-phase SO_2, i.e., less than half that predicted computationally for physisorbed SO_2 at low coverage. The discrepancy strongly suggests that the observed bands should not be attributed to direct SO_2 physisorption on MgO, but rather more likely reflect physisorption in multilayers, likely on top of a surface saturated with chemisorbed SO_2.

The two lowest frequency bands persist upon evacuation and heating to 100 °C (Figure 8c), although the 1057 cm^{-1} band center does red shift to 1032 cm^{-1}. These two bands have been assigned to surface sulfite species[7,8] which have been speculated to attach to the surface in a variety of conformations. The frequency ranges observed are entirely consistent with the computational results for the asymmetric and symmetric stretches of chemisorbed SO_2 discussed above, and we believe this to be the best available representation for "surface sulfite" on MgO.

SO_2 adsorption on MgO was also carried out at 350 °C on a different MgO sample. In this case (Figure 8d), the asymmetric SO_2 stretch band is centered at 1050 cm^{-1}, the symmetric stretch is shifted downward to 947 cm^{-1}, and an additional band is evident at 916 cm^{-1}. As discussed below, this last feature is associated with surface sulfate, likely generated by oxidation of surface sulfite by reaction with the oxide.

The vibrational spectrum of gas-phase SO_3 includes a higher-frequency degenerate asymmetric stretch and a symmetric stretch 260 cm^{-1} lower in energy.[29] The LDA again overestimates the asymmetric stretch but underestimates the symmetric stretch by ~40 cm^{-1}, so that the splitting is overestimated by 60 cm^{-1}. The source of this discrepancy is unknown. Chemisorption on the (001) surface red shifts and splits the degenerate band, the higher frequency branch corresponding to vibration of the slighter shorter S−O bond (Figure 7a) and the lower frequency branch to vibration of the other two. The symmetric band is red shifted to a much lesser extent. At the step edge (Figure 7b), the splitting of the degenerate band is even more pronounced: one of the branches, corresponding to the short S−O bond projecting from the surface, actually increases in frequency, while the other branch red shifts >100 cm^{-1}. The symmetric stretch also red shifts but to a lesser extent. Thus, the vibrational spectra of sulfate surface species are predicted to be highly sensitive to the details of adsorption (e.g., terrace vs step) even on the hydroxyl-free surface.

These computational results are most directly comparable with experiments involving direct exposure of SO_3 to MgO. In the one report we are aware of, SO_3 adsorbed on low surface area MgO produces S−O stretch bands at 1260 and 1105 cm^{-1},[28] in good agreement with the range of values predicted computationally for the asymmetric stretch modes of chemisorbed SO_3 on terraces and at steps.

Because of the difficulties associated with working with SO_3 gas, oxide sulfation is more commonly accomplished by oxidation of adsorbed SO_2 at elevated temperatures;[8,10,11] in any case, this treatment is more representative of the conditions experienced by oxide adsorbents. In this work, vibrational spectra were obtained either by exposing precalcined MgO samples to SO_2 and O_2 at 25 °C followed by heating or by exposure at 350 °C. At 25 °C, the spectrum is similar to that found in the absence of O_2, including both chemi- and physisorbed SO_2. Heating to 100 °C (Figure 9a) removes the features attributable to physisorption and leaves features consistent with chemisorbed SO_2 at 960 and 1030 cm^{-1}. Continued heating to 200 °C (Figure 9b) and 300 °C (Figure 9c) causes these surface sulfite features to decrease in intensity and new features at 1164 and 1098 cm^{-1} to appear. These changes can be attributed to the gradual oxidation of sulfite to sulfate and the formation of bulk $MgSO_4$,[11] but the broad and ill-resolved nature of the spectrum makes definitive assignment difficult.

Exposure of MgO to SO_2 and O_2 at 350 °C produces a much more feature-rich spectrum. Sharp bands are observed at 1272, 1213, 1164, 1066, and 947 cm^{-1} and are accompanied by shoulders at ~1100 and ~930 cm^{-1} and a shift to lower frequency of the hydroxyl band (Figure 10a). The observed spectrum is similar to that previously assigned to sulfate on a low surface area MgO.[11] From the results above, the bands at

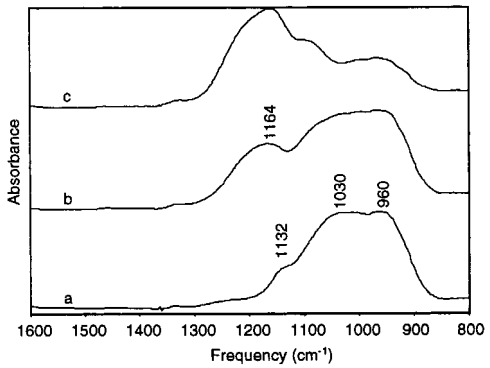

Figure 9. Observed vibrational spectra of precalcined MgO exposed to SO_2 and O_2 at room temperature: (a) after heating to 100 °C; (b) after heating to 200 °C; (c) after heating to 300 °C.

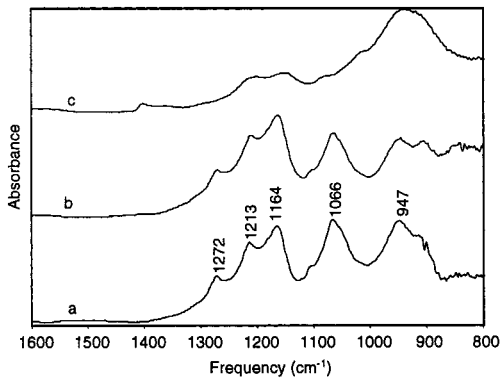

Figure 10. Observed vibrational spectra of precalcined MgO exposed to SO_2 and O_2 at 350 °C: (a) after exposure at 350 °C; (b) after heating to 400 °C; (c) after exposure to H_2 and heating to 600 °C.

1066 and 947 cm^{-1} correspond to the stretches of surface-bound SO_2 (sulfite) unoxidized by O_2. The 1272 and 1100 cm^{-1} bands correspond to those observed on SO_3-exposed MgO[28] and can be assigned to the asymmetric stretches of surface-bound SO_3 formed by oxidation of SO_2, whereas the symmetric stretches appears as a weak shoulder at 930 cm^{-1}. The 1213 cm^{-1} band also appears to be characteristic of surface-bound sulfate, possibly in an environment in which the asymmetric stretches are less strongly split. Finally, the 1164 cm^{-1} band is characteristic of bulk $MgSO_4$. As the system is heated to 400 °C (Figure 10b) the "bulk" band grows at the expense of the surface sulfite and sulfate. This trend continues upon heating to 500 °C, with the band at 1164 cm^{-1} becoming dominant. To explore the resistance to reduction of the final material, it was exposed to H_2 at 25, 100, 200, 300, 400, 500, and 600 °C. Only at the highest temperature do the 1213 and 1164 cm^{-1} sulfate features begin to diminish (Figure 10c).

Summary and Conclusions

The results presented here provide a consistent picture of SO_x chemistry on MgO. Both SO_2 and SO_3 are found through computation to combine preferentially through their sulfur centers to surface oxide anions to form what are best characterized as surface sulfite and sulfate, respectively. Reactivity is greater on coordinatively unsaturated oxide anions at step edges but is high even on the relatively unreactive MgO(001) terrace. Secondary interactions between adsorbate oxygen and surface Mg cations provide additional stability and lock the adsorbates in fixed adsorption geometries. Both SO_2 and SO_3 also weakly physisorb on the surface but convert to their chemisorbed forms with little activation energy.

Experiments to examine SO_x adsorption on MgO confirm and extend these results. SO_2 is found to chemisorb on MgO powder at room temperature to produce both surface sulfite and an overlayer of physisorbed SO_2. The latter is readily removed by evacuation at room temperature, whereas the former persists in the absence of O_2 to at least 100 °C and, by comparison of calculated and observed vibrational spectra, is consistent with the computational description for chemisorbed SO_2 and with XANES results for SO_2 adsorption on MgO.[9] SO_2 and O_2 in combination produce similar surface sulfite features upon room-temperature exposure to MgO, but exposure at 350 °C introduces additional vibrational features that can be attributed to surface sulfate and that are consistent with those predicted for chemisorbed SO_3. Simultaneously, bulklike sulfate is formed and, upon further heating, begins to predominate the observed spectra.[9]

The high affinity of SO_2 and SO_3 for even the MgO(001) surface suggests that other oxides will exhibit significant reactivity to these two. Preliminary computations confirm this to be the case for a BaO surface. This work provides qualitative insight into the nature of these interactions that should be transferable to other oxides. It also highlights the challenges confronting the design of SO_x-tolerant oxide-based catalytic materials.

Acknowledgment. We wish to acknowledge Mark Dearth of the Ford Research Laboratory for numerous helpful discussions regarding NO_x and SO_x adsorption in NO_x traps, and José Rodriguez of Brookhaven National Laboratory for generously sharing experimental and computational results prior to publication.

References and Notes

(1) Shelef, M. *Chem. Rev.* **1995**, *95*, 209.
(2) Miyoshi, N.; Matsumoto, S.; Katoh, K.; Tanaka, T.; Harada, J.; Takahashi, N.; Yokota, K.; Sugiura, M.; Kasahara, K. *Soc. Auto. Engineer.* **1995**, 950809.
(3) Parr, R. G.; Yang, W. *Density-Functional Theory of Atoms and Molecules*; Oxford University Press: New York, 1999.
(4) Payne, M. C.; Teter, M. P.; Allan, D. C.; Arias, T. A.; Joannopoulos, J. D. *Rev. Mod. Phys.* **1992**, *64*, 1045.
(5) Car, R.; Parrinello, M. *Phys. Rev. Lett.* **1985**, *55*, 2471.
(6) Brown, G. E., Jr.; Henrich, V. E.; Casey, W. H.; Clark, D. L.; Eggleston, C.; Felmy, A.; Goodman, D. W.; McCarthy, M. I.; Maciel, G.; McCarthy, M. I.; Nealson, K. H.; Sverjensky, D. A.; Toney, M. F.; Zachara, J. M. *Chem. Rev.* **1999**, *99*, 77−174.
(7) Goodsel, A. J.; Low, M. D. J.; Takezawa, N. *Environ. Sci. Technol.* **1972**, *6*, 268.
(8) Schoonheydt, R. A.; Lunsford, J. H. *J. Catal.* **1972**, *26*, 261.
(9) Rodriguez, J. A.; Jirsak, T.; Freitag, A.; Larese, J. Z.; Maiti, A. *J. Phys. Chem. B* **2000**, *104*, 7439.
(10) Babaeva, M. A.; Tsyganenko, A. A.; Filimonov, V. N. *Kinet. Katal.* **1984**, *25*, 921.
(11) Benistel, M.; Waqif, M.; Saur, O.; Lavalley, J. C. *J. Phys. Chem.* **1989**, *93*, 6581.
(12) Waqif, M.; Saur, O.; Lavalley, J. C.; Perathoner, S.; Centi, G. *J. Phys. Chem.* **1991**, *95*, 4051.
(13) Stark, J. V.; Park, D. G.; Lagadic, I.; Klabunde, K. J. *Chem. Mater.* **1996**, *8*, 1904.
(14) Pacchioni, G.; Clotet, A.; Ricart, J. M. *Surf. Sci.* **1994**, *315*, 337.
(15) Pacchioni, G.; Ricart, J. M.; Illas, F. *J. Am. Chem. Soc.* **1994**, *116*, 10 152.
(16) Kleinman, L.; Blylander, D. M. *Phys. Rev. Lett.* **1982**, *48*, 1425.
(17) Gonze, X.; Stumpf, R.; Scheffler, M. *Phys. Rev. B* **1991**, *44*, 8503.
(18) Stumpf, R.; Gonze, X.; Scheffler, M. *Fritz-Haber-Institut Research Report No. 1*; 1990.
(19) Troullier, N.; Martins, J. L. *Phys. Rev. B* **1991**, *43*, 1993.
(20) Perdew, J. P.; Zunger, A. *Phys. Rev. B* **1981**, *23*, 5048.
(21) Perdew, J. P.; Wang, Y. *Phys. Rev. B* **1992**, *45*, 13244.
(22) Perdew, J. P.; Chevary, J. A.; Vosko, S. H.; Jackson, K. A.; Pederson, M. R.; Singh, D. J.; Fiolhais, C. *Phys. Rev. B* **1992**, *46*, 6671.
(23) Wycoff, R. W. G. *Crystal Structures*; Interscience: 1963.

(24) Langel, W.; Parrinello, M. *J. Chem. Phys.* **1995**, *103*, 3240.
(25) Kantorovich, L. N.; Holender, J. M.; Gillan, M. J. *Surf. Sci.* **1995**, *343*, 221.
(26) Tasker, P. W. *Structure and Properties of MgO and Al_2O_3 Ceramics*; American Ceramic Society: Columbus, 1988; p 176.
(27) Tasker, P. W.; Duffy, D. M. *Surf. Sci.* **1984**, *137*, 91.
(28) Stark, J. V.; Klabunde, K. J. *Chem. Mater.* **1996**, *8*, 1913.
(29) Herzberg, G. *Molecular Spectra and Molecular Structure*: *Infrared and Raman Spectra of Polyatomic Molecules*; Van Nostrand: New York, 1950; Vol. 2.